Biosensors and Bioelectronics 292 (2026) 118080

Contents lists available at ScienceDirect

Biosensors and Bioelectronics

journal homepage: www.elsevier.com/locate/bios

Surface plasmon resonance unveils diffusion fingerprints of biomolecular mixtures in ocular fluid models

Damiano Calcagno [a], Valentina Oliveri [b], Maria Cristina Parravano [a], Nunzio Tuccitto [b,*], Giuseppe Grasso [b,**]

[a] IRCCS-Fondazione Bietti, Rome, Italy
[b] Department of Chemical Sciences, University of Catania, Viale Andrea Doria 6, 95125, Catania, Italy

ARTICLE INFO

Keywords:
Alpha crystallin
Surface plasmon resonance
Diffusion coefficient
Ocular model
Albumin

ABSTRACT

Analyzing diffusion processes within complex biomolecular mixtures is essential but technically challenging, especially for understanding molecular interactions in physiological environments. Here, we apply the diffusion-based surface plasmon resonance (*D*-SPR), a recent, label-free methodology that combines accurate SPR-based diffusion measurements with stochastic computational simulations, to address biomolecular complexity in ocular fluid models. By combining discrete Fréchet distance analysis with Gillespie algorithm simulations, *D*-SPR effectively detects unique diffusion patterns in binary (BSA/glycine, BSA/glucose) and ternary (HSA/ubiquitin/glycine) mixtures, enabling composition characterization without the need for external fluorophores or chromatographic techniques. Demonstrating the method sensitivity, as a proof-of-concept, we applied our workflow to probe the oligomeric transitions of bovine lens α-crystallin induced by mild acidification (pH 6.5). Our findings revealed subtle oligomer dissociation events and identified smaller, rapidly diffusing subunits, undetectable by conventional dynamic light scattering, thus providing insights into protein structural changes potentially pertinent to cataractogenesis. Considering the critical role of diffusion-based processes in eye health, the proposed *D*-SPR approach provides an advanced and versatile analytical tool with significant potential applications in medical research, especially ophthalmology.

1. Introduction

Characterizing biomolecular mixtures poses a fundamental challenge in medical research, biochemistry, omic sciences, and drug development (Pan et al., 2024; Tang and Chen, 2023). This task is indeed crucial for comprehending molecular pathways in diseases and for elucidating different key molecular mechanisms, with the goal of developing new treatment plans. Among the many biological fluids of interest, ocular fluids are a highly informative and clinically significant target. Their meticulous monitoring is pivotal for the health of the eye, the most critical and complex sensory organ in the human body. Because of its unique structure and the highest water content by volume among all organs, several primary ocular functions and regulations rely on diffusion mechanisms (Cholkar et al., 2013; Fu et al., 2020; Stamer et al., 2008). In this regard, it was observed that a dysregulation of oxidative stress biomarkers (malondialdehyde (MDA), 4-hydroxynonenal (HNE)), inflammatory cytokines (interleukin-1β (IL-1β), interleukin-6 (IL-6), and tumor necrosis factor-alpha (TNF-α)), angiogenic factors (vascular endothelial growth factor (VEGF)), and proteases (matrix metalloproteinase-9 (MMP-9), cathepsins), occurring in aqueous humor (AH), vitreous humor (VH) and tears, could be an early warning indicator of ocular inflammation, or, in the most severe cases, chronic and degenerative pathological conditions such as dry eye disease (DED) (Fu et al., 2020), glaucoma (Aranaz et al., 2022; Sanchez et al., 2025), or diabetic retinopathy (DR) (Loukovaara et al., 2017; Midena et al., 2021).

In this work, we describe a new method for analyzing biomolecular mixtures using a combined approach based on Diffusion-based Surface Plasmon Resonance (*D*-SPR) (Zingale et al., 2023) and an in silico framework that features a numerical simulation model of particles flowing through a virtual microfluidic environment (Calcagno et al., 2025). Classical SPR has emerged as a versatile and powerful optical technique that enables real-time, label-free detection of biomolecular interactions, providing kinetic and affinity data (Bellia et al., 2019; Distefano et al., 2022; Grasso et al., 2009a; Homola, 2008). Over the past

* Corresponding author.
** Corresponding author.
E-mail addresses: n.tuccitto@unict.it (N. Tuccitto), grassog@unict.it (G. Grasso).

https://doi.org/10.1016/j.bios.2025.118080
Received 22 August 2025; Received in revised form 6 October 2025; Accepted 7 October 2025
Available online 14 October 2025

decades, it has found widespread applications in diverse fields such as clinical diagnostics, environmental monitoring, food safety assessment, and the development of advanced nanomaterials (Mariani and Minunni, 2014; Masson, 2020). Recently, we assessed the diffusion coefficient (*D*) of molecules in solution using this novel approach, ranging from heavy water to albumin in different conformations and insulin in various aggregation states (Calcagno et al., 2024, 2025; Zingale et al., 2023). *D*-SPR is a cutting-edge analytical technique that uses the optical properties of SPR to analyze the diffusion properties of molecules (Basile et al., 2024), especially biomolecules in solution (Basile et al., 2025). Specifically, the method enables the precise determination of the apparent *D* of substances in a microfluidic environment, revealing valuable information about the molecular conformation and oligomeric states of the analyzed species (Calcagno et al., 2024, 2025).

In detail, our study addresses the feasibility of monitoring binary and tertiary biomolecular mixtures and how these can be potentially affected by "pathogenic" stimuli, enabling us to properly assess structural modifications and oligomerization states of proteins or biomolecules. Our liquid eye model systems include proteins such as human serum albumin (HSA), bovine serum albumin (BSA), ubiquitin (Ub), and amino acids like glycine or sugars like sucrose. These molecules are broadly involved in eye homeostasis, and variations in their concentration could trigger an alert signal. As evidence of this, due to an enhanced permeability of the hemato-aqueous barrier, higher levels of HSA have been found in the AH of patients with glaucoma coupled with pseudoexfoliation syndrome when compared to the control pool (Moreno-Montañés and Blesa, 1995). Ubiquitin is a tag protein that plays a key role within the Ubiquitin-Proteasome system (UPS), which is responsible for the maintenance of cellular proteostasis (Tundo et al., 2020). In the context of the eye, due to oxidative stress, an accumulation of high-mass ubiquitin conjugates in bovine lens epithelial cells was detected, leading to altered proteolytic pathways (Shang and Taylor, 1995). Glycine supplementation shows protective effects against retinal damage induced in diabetic rats and restores the glycine-serine pathway in patients affected by macular telangiectasia (MacTel) (Gholami et al., 2019; Lim et al., 2024).

Moreover, as a case study, we investigated bovine lens α-crystallin to assess its oligomeric organization following a pH change, simulating a pathological acidosis condition (Dmitriev and Linsenmeier, 2025; Dreffs et al., 2018).

This is particularly relevant because α-crystallin, one of the major protein components of the lens, is responsible for its transparency and structural sustenance. Moreover, it is classified within the small heat shock protein family (sHSPs), and its chaperone activity, regulated by its multimeric organization, can prevent protein unfolding or aggregation caused by thermal shock or cellular oxidative stress (Andley, 2007; Sprague-Piercy et al., 2021).

Analytical methods have gradually advanced in resolving biomolecular mixtures, but none have reached the final development stage. Consequently, several approaches, from spectroscopic to sophisticated machine learning algorithms, have been implemented, each providing advantages and drawbacks (He et al., 2019; Valeja et al., 2015). Size-exclusion chromatography (SEC), reversed-phase chromatography (RPC), and ion-exchange chromatography (IEC), all based on chromatographic principles, are often used in characterizing biological fluids. They offer high-resolution results, but, on the contrary, disaggregation of supramolecular complexes, protein denaturation, or sample loss may occur during the chromatographic run (Chelius and Bondarenko, 2002; Lee and Chang, 1996; Zhai et al., 2024). Furthermore, the above-mentioned techniques suffer from a time-consuming workflow for sample preparation, limited sensitivity for low-abundance proteins, and insufficient resolution of closely related species (Lebendiker, 2024; Winther and Reubsaet, 2005). Mass spectrometry (MS), on the other hand, offers sensitivity and specificity (Grasso et al., 2009b). For instance, native MS enables the study of intact biomolecular complexes without denaturation, thereby preserving their oligomeric states; however, its resolution decreases for species exceeding 30 kDa and for complex mixtures (Zhai et al., 2024). Nanoflow ion-exchange chromatography-native mass spectrometry (nSCX-nMS) has proven effective in characterizing more complex proteoforms under native conditions, but it faces limitations due to signal suppression and desolvation issues, necessitating advanced instrumentation and sophisticated data analysis (Zhai et al., 2024). Nuclear Magnetic Resonance (NMR) spectroscopy has emerged as a powerful tool for studying diffusion processes in various systems, from simple liquids to complex biological tissues. However, it requires sophisticated and costly instrumentation, deuterated solvents, or isotopically labeled molecules, which are far from physiological conditions (Björnerås et al., 2014; Rajagopalan et al., 2004). Other advancements have introduced integrated and emerging approaches that enhance biomolecular resolution. For example, Capillary electrophoresis (CE) can separate biomolecules based on electric fields and offers an effective strategy for isolating small amounts of proteins in biological samples. However, it requires meticulous optimization, and achieving reproducibility can be challenging due to fluctuations in electroosmotic flow and capillary surface interactions (Zhang et al., 2021). Eventually, Taylor Dispersion Analysis (TDA) has become a powerful tool for characterizing the properties of mixtures under laminar flow conditions, particularly in determining *D* and hydrodynamic radii of components within a mixture (Cottet et al., 2007; Taylor, 1953). This provides insights into the behavior of individual components and their interactions (Latunde-Dada et al., 2015). However, traditional TDA is restricted to detecting ultraviolet-absorbing or fluorescent compounds, or it requires the addition of fluorophores for effective detection when the sample lacks native fluorescence (Somnin et al., 2024).

To improve the current techniques portfolio and overcome the above-reported limitations, we propose *D*-SPR and in-silico analysis for profiling binary and ternary mixtures in aqueous solutions. While this technique has shown strong potential in characterizing individual species, its application to analyzing multicomponent systems remains largely unexplored. Nevertheless, due to its high sensitivity to subtle changes in refractive index, the *D*-SPR approach holds promise for enhancing resolution capabilities. Moreover, by integrating it within an in-silico framework, we aim to enhance the resolving power for characterizing and deconvoluting physiological multicomponent systems, such as biological fluids and, in particular, ocular liquid tissues.

2. Results and discussion

2.1. Stochastic modeling of molecular mixtures in a microfluidic channel

The theory describing molecular diffusion and transport in a microfluidic channel is based on the diffusion-advection equation, which can be solved numerically by stochastic approaches. Among these, Gillespie's algorithm is a particularly effective tool for modeling chemical-physical processes governed by the intrinsic randomness of molecular motion (Calcagno et al., 2025). The simulation operates on a reduced two-dimensional domain, in which the longitudinal coordinate X(t) represents the motion along the channel axis, while Y(t) describes the radial position within the cross section. The local convective velocity along X is a parabolic function of Y, in agreement with the classical solution of the velocity profile for laminar flow in the Hagen-Poiseuille regime:

$$X(\mathrm{Y}) = \frac{\Delta \mathrm{P}}{4\,\eta\,\mathrm{L}}\left(\mathrm{R}^2 - \mathrm{Y}^2\right) \tag{1}$$

where ΔP represents the pressure gradient, η the dynamic viscosity, L the length of the section considered, and R the radius of the channel. This convective component is calculated instant by instant for each particle as a function of its current transverse position. In this section, the term "particles" refers specifically to non-interacting, point-like

random walkers that represent analyte molecules in our stochastic diffusion model. At each discrete time interval Δt, the position of each particle is updated by summing a deterministic term, associated with the local hydrodynamic drift, and two stochastic terms, associated with Brownian diffusion along both spatial directions. The updating equation therefore results:

$$X(t+\Delta t) = X(t) + V_X(Y(t))\cdot\Delta t + \sqrt{2D\Delta t}\cdot\mathcal{N}_{\mathcal{X}}(0,1) \quad (2)$$

$$Y(t+\Delta t) = Y(t) + \sqrt{2D\Delta t}\cdot\mathcal{N}_{\mathcal{Y}}(0,1) \quad (3)$$

where D represents the molecular diffusion coefficient, and $N_{(X)}$ (0.1) $N_{(Y)}$ (0.1) are independent Gaussian random variables with zero mean and unit variance. To prevent particles from moving beyond the geometric boundaries of the channel, a reflective boundary condition was implemented, based on a geometric masking algorithm using polygons that prevent movement beyond the allowed domain. The simulation setup was parameterized with a high statistical numerosity ($P = 10^6$ particles per simulation) and with a total integration time long enough to cover the entire transport process up to the detector located downstream of the channel. In order to handle the high volume of generated

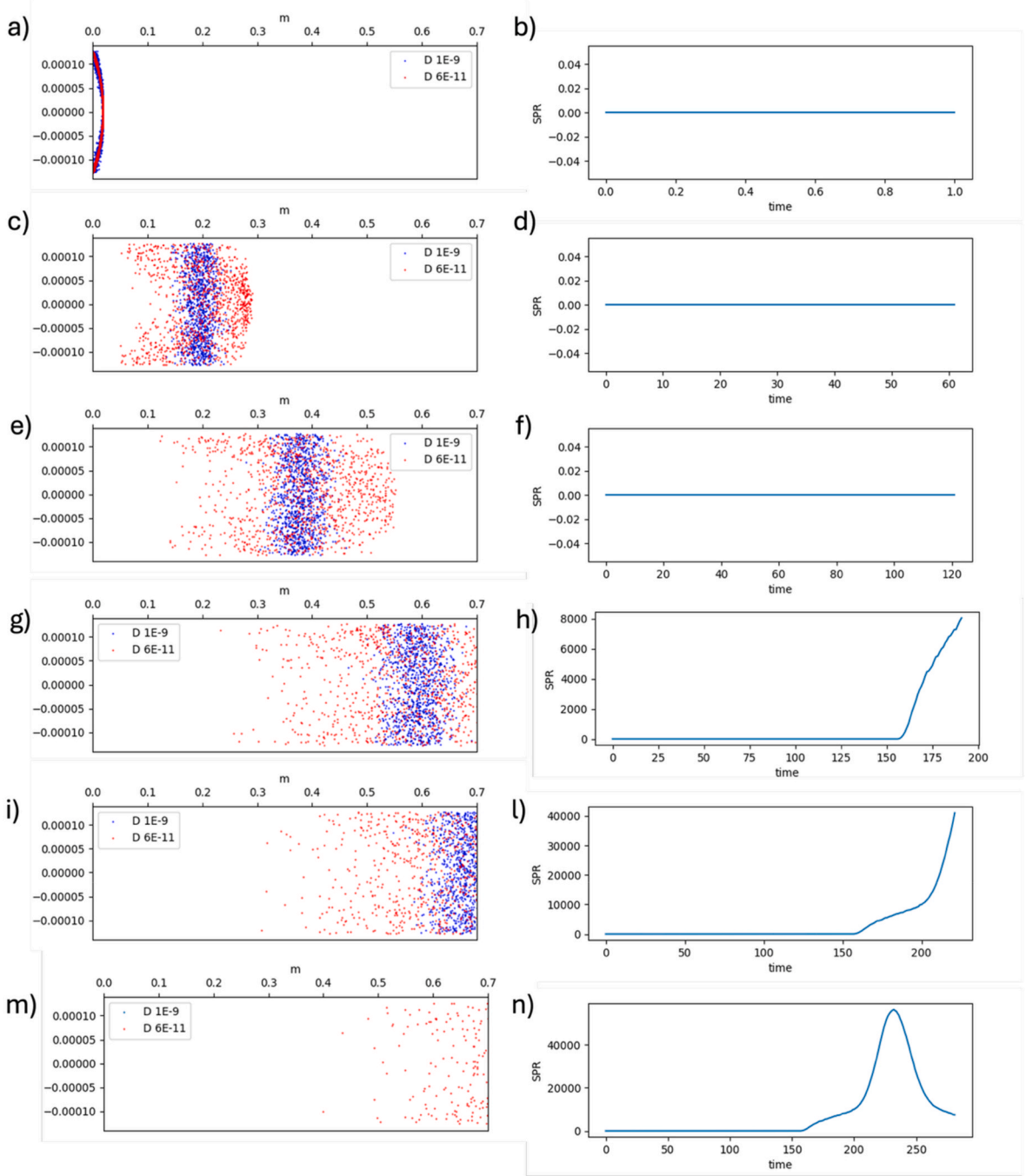

Fig. 1. Graphical representation of the stochastic simulation of transport and diffusion of two molecular species characterized by different diffusion coefficients ($D = 1 \times 10^{-9}$ m^2/s in blue and $D = 6 \times 10^{-11}$ m^2/s in red) along the microfluidic channel. Shown on the left (panels a, c, e, g, i, m) is the time evolution of the spatial positions of the particles at the indicated times: (a) 0 s, (c) 60 s, (e) 120 s, (g) 190 s, (i) 220 s, (m) 280 s. On the right (panels b, d, f, h, l, n) is the corresponding simulated SPR signal, expressed as the cumulative fraction of molecules detected by the detector positioned at the end of the channel as time progresses. (For interpretation of the references to color in this figure legend, the reader is referred to the Web version of this article.)

data, the simulation data are progressively saved to files in HDF5 format, enabling efficient subsequent analysis of both spatial distributions and simulated SPR signals. The entire simulation scheme thus explicitly and realistically reproduces the transport-diffusion process in the laminar regime of molecular mixtures characterized by different *D* values, allowing the extraction of both qualitative information on the evolution of diffusive fronts and quantitative predictions on the SPR signals detected downstream. A pseudo-code of the algorithm is provided in the "supporting information", whereas some videos of simulated signals from various mixtures are also provided as supplementary material.

In the simulations performed, for reasons of computational effort, the "tight plug" mode was adopted, in which the initial position of the particles was randomly distributed in a small portion of the tube, as shown in Fig. 1a. Considering the purpose of the mixture study, both types of particles with different *D* were "injected" simultaneously into the same initial area, while maintaining a random spatial distribution. The initial positions thus defined evolve over time under the combined influence of diffusion (described by the *D*) and the parabolic flow profile (Hagen-Poiseuille law). The simulations (Fig. 1b and c) clearly show that molecules with different *D* form different interfaces along the channel: compounds with high *D* (e.g., small molecules such as glycine, with *D* of the order of 1E-9 m^2/s) exhibit a compact and nearly Gaussian concentration profile, while larger molecules (such as human serum albumin, HSA, with *D* of the order of 6E-11 m^2/s) show a broader and more asymmetric distribution. Fig. 1 shows the simulated SPR signal considering the detector positioned at the end of the microfluidic channel with a sampling depth of 15 % of the tube diameter. The sampling depth value acts as a calibration factor to optimize the fit between the simulated curves and the experimental data, as reported earlier (Calcagno et al., 2025). The spatial and temporal evolution clearly highlights how the differential diffusion results in the progressive separation of the fronts of the two molecular populations: the higher diffusivity species (blue) tends to maintain a relatively narrow Gaussian profile, while the slower diffusing species (red) shows a progressive and asymmetric broadening of its distribution. In the lower panels, particularly from g-h down to m-n, the differential contribution of the two populations also becomes explicit in the SPR signal. At this late stage, the detector initially records an increasing contribution of the slower diffusing (red) species, which anticipates the arrival of the main front. Next, the contribution of the higher diffusing species (blue) emerges, generating a narrower, symmetric peak in the SPR trace (visible at the maximum in panel n). After the appearance of the peak associated with the major *D*, the residual contribution of the lower scattering population continues to accumulate, eventually reaching the sensitive zone of the detector over longer times. Taken together, the simulated traces show that the SPR signal obtained in the presence of mixtures is the result of a complex convolution between the differential arrival times of the species, governed by their respective *D*. Though the system does not allow a clean separation between the two species (due to the insufficient number of theoretical plates), the overall shape of the signal still provides valuable information about the simultaneous presence of multiple molecular populations with different diffusive mobility. This result is particularly significant because it suggests that the method can be used effectively to investigate complex mixtures in their physiological state, without the need to alter their structure or functionality. In Fig. 2, the simulated *D*-SPR total curves for model mixtures comprising a fast and a slow molecular species are reported. In the absence of the fast molecule (0 % fraction), the profile exhibits a gradual ascent and prolonged tailing, characteristic of the slow-spreading species. As the fast molecule fraction increases, a narrower and more symmetrical peak appears progressively, associated with the rapid advance of the higher *D* species. Under intermediate conditions (50 %), the curve clearly shows the coexistence of the two contributions: a faster initial rise followed by an asymmetry reflecting the long-tail generated by the residual simulated slow species. Analysis of the shape of the simulated SPR signal suggests the possibility of extracting quantitative information about the

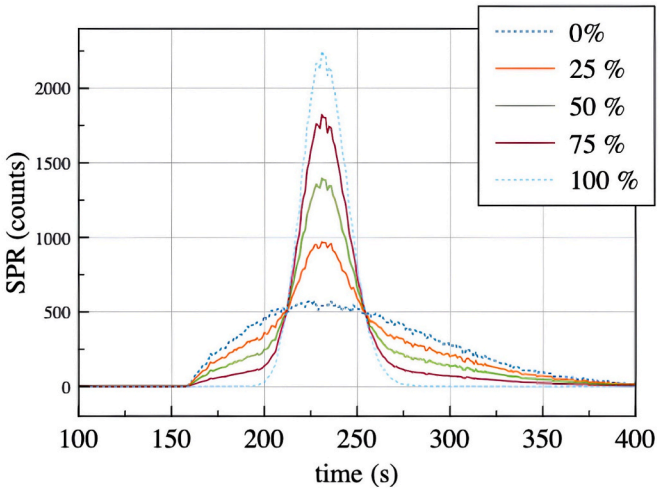

Fig. 2. Stochastic *D*-SPR simulations of the evolution of the SPR signal for mixtures of two species with distinct diffusion coefficients ($D = 1 \times 10^{-9}$ m^2/s and $D = 6 \times 10^{-11}$ m^2/s), as the relative molar composition changes. For each simulation, the total number of injected particles was kept constant by varying the mole fraction of the fast-diffusing species at 0 %, 25 %, 50 %, 75 % and 100 %, respectively. SPR traces are obtained considering a sampling depth equal to 15 % of the channel diameter and a detector positioned at the end of the microfluidic path.

composition of the mixture by exploiting morphological parameters such as the position of the maximum, skewness, width at mid-height, and tail extension. Such observables open the way for potential quantitative applications of experimental *D*-SPR in the study of complex systems, including protein degradation processes, conformational changes, and biochemical reactions.

To further extend the potential of the simulative *D*-SPR method, simulations were conducted on multicomponent systems beyond the simple binary mixtures previously discussed. In Fig. S1A, the simulated SPR signal obtained by injecting an equimolar ternary mixture consisting of three representative species with $D = 1 \times 10^{-9}$ m^2/s (small-molecule model such as glycine), $D = 6 \times 10^{-11}$ m^2/s (albumin-type protein model), and $D = 1.5 \times 10^{-10}$ m^2/s (intermediate, modeling a system such as ubiquitin) is presented. The superposition of the three contributions results in a complex shape of the SPR signal, characterized by a rapid initial rise due to the more mobile species, a second, relatively symmetric intermediate contribution, and finally a more prolonged tail associated with the slow diffusion component. This result confirms the method's ability to detect and distinguish multiple contributions, as in the presence of multiple coexisting species. Fig. S1B further extends the concept by modeling a more realistic multicomponent system for polydisperse materials, such as natural or synthetic polymers characterized by non-monodisperse molecular weight distributions. In this case, the injection of a mixture consisting of 6 distinct populations, each with its own *D* value, distributed according to the concentration function shown in Fig. S1C, characterized by various D fractions, was simulated. The result shows a highly smoothed SPR signal, without abrupt inflection points, resulting from the continuous convolution of overlapping diffusive contributions. This type of signal, although it does not allow direct resolution of individual components, maintains relevant information about the overall distribution of diffusive coefficients, indicating the potential for statistically reconstructing the underlying diffusive distribution through numerical deconvolution or advanced fitting.

2.2. Fitting model of molecular mixtures using diffusion-based surface plasmon resonance (D-SPR)

We develop a mathematical fitting model that describes the total 1st derivative SPR signal of a multicomponent mixture (binary, ternary, or

N-component) as the sum of its individual contributions. To implement the model, we incorporated instrument factors in the form of a constant $k = \alpha \times \delta$, where α is the detector sensitivity and δ refers to the penetration depth of the flow cell, which depends on the evanescent field of the SPR gold sensor (Calcagno et al., 2025). Therefore, to provide a semi-quantitative description of the multicomponent systems studied, we define the following equation:

$$S(t) = k\sum_{i=1}^{N}[c_i \cdot \gamma_i \cdot R_i(t)] \quad (4)$$

where N is the number of species in the mixture, c_i is the concentration of the *i-th* component, and γ_i is the refractive-index increment $\left(\frac{dn}{dc}\right)$ which characterizes how strongly that species alters the refractive index, and consequently the instrument response (in $mL \cdot g^{-1}$). The function $R_i(t)$ is the unit-normalized 1st derivative *D*-SPR response of component *i*, encoding its diffusion-governed transport profile, while k unifies instrument parameters like detector sensitivity and sampling depth into a single calibration constant. The resulting $S(t)$, reported in 1st derivative response units, therefore captures the summed, weighted contributions of all molecular populations over time, as illustrated in Fig. 3. This model is valid under the following assumptions: no interaction occurs between components, and there is no viscosity mismatch between the running buffer and the samples. The total signal is linear in both concentration and refractive index increment, and eventually, the shape of each contribution $R_i(t)$ depends on its diffusion coefficient D_i, temperature, and flow rate.

When not all components of the mixture are known, one or more deconvolution steps can be performed to identify the different contributions of the overall signal. This method is not recommended when there is limited understanding of the system, as it can lead to misinterpretation of the data.

2.3. Mixture diffusion analysis through D-SPR approach

The *D*-SPR approach was originally developed for studying the *D* of single molecules (Zingale et al., 2023, 2024), to determine their hydrodynamic radius and, consequently, their conformational and/or aggregation state (Basile et al., 2024, 2025, 2024; Calcagno et al., 2024, 2025). Thanks to the optical properties of SPR, which can detect very small differences in refractive index, and our experimental setup (including an in-silico framework), we are able, for the first time, to advance the resolution of diffusion profiles in binary and ternary biomolecular mixtures. The biomolecular mixtures used in this liquid eye model are well-characterized and play a crucial role in biological systems, thereby enabling the creation of a more realistic physiological environment.

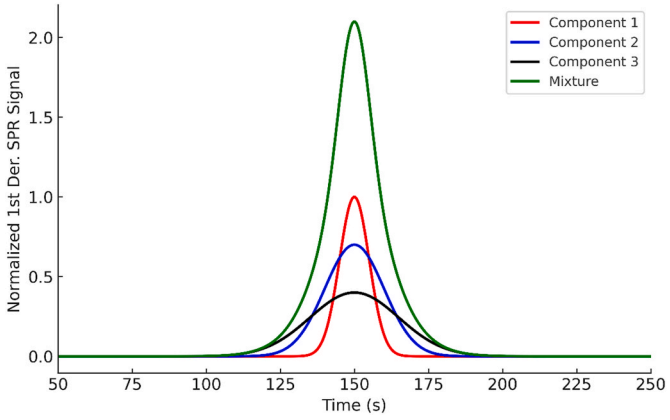

Fig. 3. Graphical representation of a simulated ternary mixture (green solid line), composed of three molecular species with different *D* values, obtained through a *D*-SPR measurement along the microfluidic channel. Component 1, with the highest D, is shown as a solid red line; component 3, with the lowest D, as a solid black line; and component 2, with an intermediate D, as a solid blue line. According to equation (4), the sum of the individual components gives the total 1st derivative SPR signal over time. (For interpretation of the references to color in this figure legend, the reader is referred to the Web version of this article.)

The first example of a binary biomolecular system is shown in Fig. 4, which reports the BSA/Glycine mixed solution at different concentration ratios. The raw SPR signals (left panel) show an increasing slope from the 100 % BSA solution to the 100 % glycine solution, which is reflected in the first derivative signals (right panel) as a narrower and sharper signal for glycine and a broader, skewed signal for BSA. The mixed signals, composed of portions from both stock solutions, exhibit contributions from each, with a central peak originating from glycine and broader lateral heads and tails resulting from BSA, as predicted by our simulations (Fig. 2) and mathematical model.

Fig. 5 (Panels A and B) show detailed views of the 1st derivative SPR signals for the 50/50 % solution of BSA and glycine, and the 50/50 % BSA plus glucose solution, respectively. Specifically, we demonstrate that the signals related to the binary mixtures are an exact overlap of the combined singular contributions, aligning with our earlier models.

Based on the measurements performed and reported in this paper, we demonstrate that the total 1st derivative signal of a mixture is given by the arithmetic sum of its individual components, provided that no interaction occurs between them, as well as with the gold surface of the SPR system. Under these conditions, as predicted by our mathematical model, it is possible to assess the quantitative composition of the mixture if the refractive index increment $\left(\frac{dn}{dc}\right)$ of the injected molecules is known. On the contrary, when the model assumptions are not respected, we can observe a distortion of the molecules' Gaussian profiles, a shift in the peaks, or a change in intensities in the 1st derivative signals. This counter-effect could be potentially monitored and rationalized to study molecules reacting in solution or with the surface; however, these phenomena will be a matter for further technique developments and implementation.

The liquid model systems developed in this study were validated not only in a binary mixture but also extended to a ternary system (Fig. 5, Panel C) consisting of equal weight/volume percentages of human serum albumin (HSA), ubiquitin, and glycine dissolved in phosphate-buffered saline (PBS) at pH 7.4. This strategy offers a new framework for investigating increasingly complex and physiologically relevant biomolecular systems.

2.4. Acidosis changes the oligomerization state of α-crystallin detected by D-SPR

α-crystallin is a major small heat shock protein (sHSP) and a key molecular chaperone found abundantly in the vertebrate eye lens, where it plays a pivotal role in maintaining lens transparency by preventing the aggregation of other structural proteins (Sprague-Piercy et al., 2021). It consists of two homologous subunits, αA and αB, which assemble into large, heterogeneous oligomeric complexes (Sprague-Piercy et al., 2021). These oligomers vary in size and composition, with αB-crystallin often forming 24-mers, and hydrodynamic studies reporting diameters ranging from 18 to 22 nm for the α-crystallin mixture (Peschek et al., 2009). The pH of the surrounding environment has a critical effect on α-crystallin structure, oligomeric stability, and, consequently, its chaperone activity. At acidic pH, especially below pH 3.5, a transition occurs where αB subunits tend to dissociate and unfold, while αA subunits remain largely folded and associated (Rasmussen et al., 2011).

Maintaining the appropriate oligomeric structure and chaperone function of alpha-crystallin is crucial in preventing protein aggregation, a central event in cataractogenesis, the leading cause of preventable blindness worldwide (Andley, 2007). Pathological pH changes in the

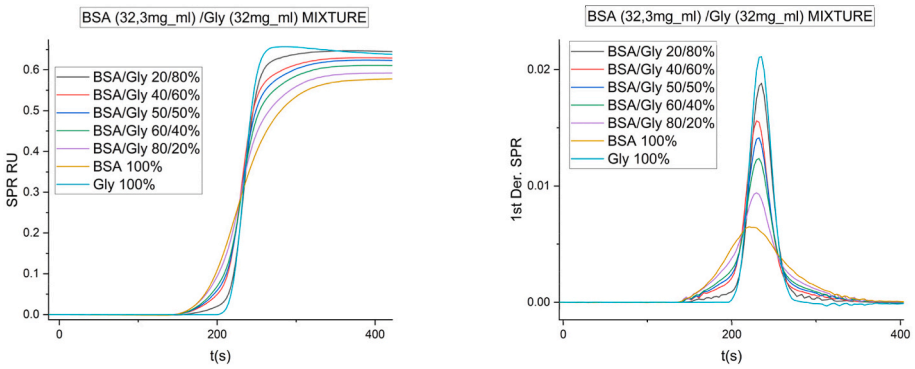

Fig. 4. BSA/Glycine experimental mixtures SPR curves (left) and the first derivatives (right) at different concentration ratios (% w/v) in PBS 10 mM at pH 7.4.

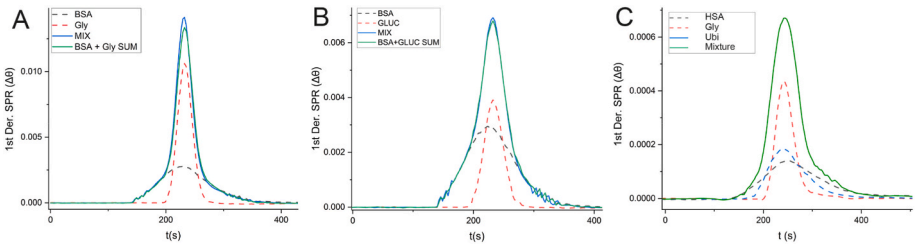

Fig. 5. *Panel A*: 1st derivative SPR curves of BSA/Gly mixture (50/50 % w/v): the black and red dashed lines represent the single 50 % dilutions of BSA and glycine, respectively; the blue solid line shows the mixture solution curve, while the green solid line depicts the mathematical sum of the two single dilutions. *Panel B*: 1st derivative SPR curves of BSA/Glucose mixture (50/50 % w/v): the black and the red dashed lines represent the single curve of BSA and Glucose, respectively; the blue solid line represents the mixture curve, while the mathematical sum of the two single concentrations is depicted in green. *Panel C*: 1st derivative experimental SPR curves of the ternary model made by HSA/Ubiquitin/Glycine mixture (33 %/33 %/33 %): the black, blue, and red dashed lines represent the individual curves of HSA, Ubiquitin, and Glycine, respectively, while the dark green solid line represents the ternary mixture curve. (For interpretation of the references to color in this figure legend, the reader is referred to the Web version of this article.)

eye, such as retinal acidosis associated with diabetes (Dmitriev and Linsenmeier, 2025), can disrupt this delicate balance. However, the oligomeric state of α-crystallin remains incompletely characterized primarily due to the limitations of earlier analytical techniques, which lacked the sensitivity to detect monomers or smaller oligomeric species if larger aggregate species are concurrently present.

For this reason, applying our *D*-SPR approach, we tried to assess the α-crystallin structure and oligomeric stability at acidic pH to mimic pathological acidosis conditions. First, a physiological solution of α-crystallin at pH 7.4 (Fig. 6, left panel) was analyzed to have a direct measurement of the *D* of the oligomeric complexes expected under these conditions. Consequently, a hydrodynamic radius was calculated using the Stokes-Einstein equation, and the resulting values are reported in Table S1. Additionally, dynamic light scattering (DLS) was also performed to obtain another independent measurement (Figs. S3 and S4 of the Supporting Information) and to compare the results.

To explore acidic conditions that mimic a pathogenic stimulus and determine if the sample oligomeric composition changes, we prepared a pH 6.5 solution (Fig. 6, right panel) and performed the same analyses, reporting the obtained values in Table 1S. In this case, the multicomponent fitting is not reported to avoid speculations. However, our *D*-SPR calculation, based on experimental curves, showed that the global *D*-value for pH 7.4 is $2.10 \cdot 10^{-11}$ m^2/s, while for pH 6.5 it is $2.82 \cdot 10^{-11}$ m^2/s. When converted to average hydrodynamic radius, the values are 11.70 and 8.71 nm at pH 7.4 and pH 6.5, respectively (Fig. S2 and Table S1). If we consider the average *D* derived from *D*-SPR, the observed trend, with an increase in global *D*-value at acidic pH, indicates an actual overall decrease in hydrodynamic radius, in contrast with the DLS data reported in Table S1. This apparent discrepancy arises from fundamental differences in the detection principles of the two techniques: *D*-SPR integrates contributions from all species in solution, including small oligomers or dissociated subunits, whereas DLS is heavily biased toward larger molecules, which scatter more intensely and effectively mask the presence of smaller components. Consequently, *D*-SPR is more sensitive to early oligomeric dissociation events that precede measurable changes in size distribution by DLS.

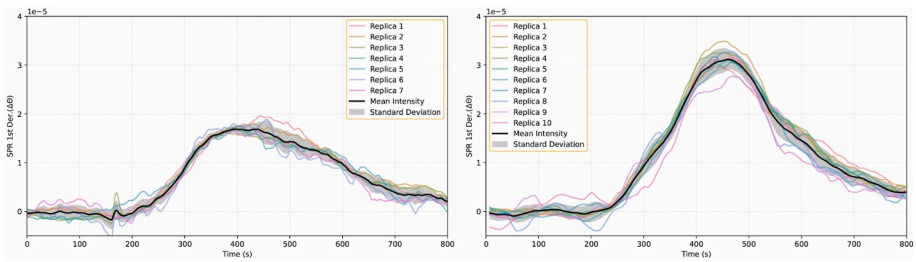

Fig. 6. The 1st derivative SPR experimental curves of the α-crystallin solution (0.5 mg/ml in PBS 10 mM) obtained at pH 7.4 (left panel) and pH 6.5 (right panel); multicolor lines are referred to the various replicas injected at 5 μl/min; the black line is the mean value between replicas, while the grey shadow indicates the standard deviation of all replicas.

A detailed analysis of the diffusion curves reveals notable differences between the acidic (pH 6.5) and physiological (pH 7.4) solution conditions (see Fig. S2). Specifically, under physiological conditions, the α-crystallin diffusion profile deviates from its characteristic pseudo-Gaussian distribution, giving rise to a distinctly bimodal signature. As previously described, this mixed diffusion profile is marked by the emergence of an additional central peak, indicative of a population with a higher *D* value at pH 6.5. This is accompanied by a modest broadening of the peak corresponding to species with lower diffusivity. The literature reports several models of α-crystallin quaternary dynamics that account for its structural plasticity, with proposed exchange units ranging from individual monomers to dimers and even dimers of dimers (Baldwin et al., 2011; Bova et al., 2000; Inoue et al., 2021; Van den Oetelaar et al., 1990). Considering this evidence, it is likely that the higher average *D* values at pH 6.5 indicate the dissociation and reorganization of smaller oligomeric subunits, which are missing under physiological pH conditions and are too small to be detected by DLS. Conversely, the broadening of the lower diffusion peak suggests a slight increase in hydrodynamic radius, consistent with DLS measurements and indicative of modest oligomeric expansion or aggregation under mildly acidic conditions.

Such a structural reorganization observed under mildly acidic conditions (pH 6.5) may indicate a quick response to a pathological stimulus, and this oligomerization transition could be relevant to disease states within ocular tissues, such as mechanisms involved in the development of cataract or similar age-related or degenerative eye disorders. Contributing to the understanding of this conformational rearrangement at the molecular level may therefore offer valuable insights into the mechanistic basis of protein misfolding or aggregation events that contribute to ocular pathophysiology.

3. Conclusions

The *D*-SPR methodology described here provides a robust, label-free approach to characterizing the diffusion patterns of biomolecular mixtures under biologically relevant conditions. By combining accurate diffusion measurements with stochastic computational modeling, this method effectively overcomes challenges in resolving and characterizing mixtures without disrupting native molecular states or relying on labeling and chromatography separation. A selection of biomolecules involved at various levels in ocular homeostasis has been used to validate the proposed mathematical model. Specifically, human and bovine albumin, ubiquitin, glycine, and glucose have been combined in binary and ternary systems dissolved in physiological buffer to mimic ocular fluids. A detailed analysis of these systems using our *D*-SPR approach showed strong agreement between experimental results and simulation predictions, confirming the method's accuracy and reliability.

After refining the methodology, we extended it to α-crystallin, demonstrating the method's ability to detect subtle, physiologically relevant oligomeric rearrangements that are otherwise undetectable by traditional analytical techniques. This provides valuable insights into eye-related pathophysiological processes. Future enhancements in quantitative capability, application to more complex biological systems, implementation of optical designs such as nearly guided-wave or ultralong-range SPR to extend the penetration depth and effective probing range (e.g., whole-cell analysis) (Bajaj et al., 2023; Shrivastav et al., 2021), and integration with complementary analytical methods will further increase *D*-SPR's impact, fostering new discoveries in biomedical research, clinical diagnostics, and therapeutic development.

4. Experimental section

4.1. Materials

Human Serum Albumin (HSA, recombinant, expressed in rice, lyophilized powder, purity ≥96 %, CAS: 70024-90-7) and sodium hydroxide (flakes, MW: 40.00 g/mol, purity 97 %, CAS: 1310-73-2) were purchased from Sigma-Aldrich. Human Ubiquitin lyophilized powder was synthesized and purchased from Biorad; Bovine serum albumin (BSA, lyophilized powder, crystallized, MW: 66430.3 g/mol, purity ≥98 %, CAS: 9048-46-8) was purchased from Thermo Scientific. Phosphate buffer saline (PBS tablets, pH 7.4) was purchased from Oxoid Ltd, UK. 20K mPEG-SH, lyophilized powder, was purchased from Laysan Bio Inc., USA. Hydrochloric acid (MW: 36.46 g/mol, fuming≥ 37 %, CAS: 7647-01-0) was purchased from Honeywell Fluka. Glycine and Sodium dodecyl sulfate (SDS) were purchased from Carlo Erba.

4.2. D-SPR instrumental setup

The diffusion-based surface plasmon resonance measurements, referred to as *D*-SPR, were performed using a commercial angular multiparametric BioNavis SPR Navi 210A equipped with a SPR102-AU gold sensor chip (20 mm long, 12 mm wide, and 0.55 mm thick), as detailed earlier (Zingale et al., 2024). In this particular case, the gold sensor chip used is smooth and flat because nanostructured metals, nanoporous, or grating structures, as reported earlier (Isaacs et al., 2019; Shalabney et al., 2009), could increase the system's overall sensitivity but may also cause undesirable nonspecific adsorption, leading to sample loss and distortion of the diffusion curve. Additionally, to enhance antifouling properties and prevent nonspecific adsorption or interaction of the analyte with the surface, the gold chip was grafted with a PEG layer as previously reported (Svirelis et al., 2022). In this procedure, which we properly modified to improve its effect, the chip sensor was previously cleaned with 1 % SDS aqueous solution, then put into a UV/Ozone cleaner for 1 h, and immersed in a solution of mPEG-SH 20K (Laysan Bio, Inc., 2.2 mg in 10 ml of 0,9M Na_2SO_4) under agitation overnight. Before the analysis, each solution underwent sonication in an ultrasonic bath for 1 min to homogenize and remove residual air. The instrument was set to record an SPR response point every 1.87s, setting the angular range from 60 to 75°. To allow the proper diffusion of molecules, the original 35 cm injection tubings were replaced with 70 cm ones. The temperature in all measurements was set to 25 °C, and the flow rate of the injected solutions was set at 10 μL/min, except for the α-crystallin measurements, where the flow rate was set to 5 μL/min. To describe in detail the diffusion process of the sample, we start with the sample plug (200 μl) taken from the vial using a syringe pump and loaded into a sample loop. Then, this sample plug, through a Rheodyne switching valve, is positioned between the flowing buffer and directed into the 70 cm injection tubing, where diffusion effectively occurs. Once the plug reaches the SPR detector, the change in refractive index is detected and recorded into a sensogram using the Bionavis SPR-Navi Control software. The curves are then extracted in txt format with the SPR-Navi Data Viewer software. Origin software was used to graph the SPR curves and their respective first derivative signals (calculated using the same software), while the Seaborn library in Python was employed for α-crystallin. Eventually, for calculating the diffusion coefficients of α-crystallin, the experimentally obtained diffusion curves (organized in an Excel file) are analyzed using a Python script (included in the supplementary materials) that compares them to a simulated dataset through the Discrete Fréchet distance, aiming to enhance overall resolution and interpretability, as previously reported (Calcagno et al., 2025).

4.3. Dynamic Light Scattering

Dinamic light scattering (DLS) and subsequent hydrodynamic size measurements were conducted using a Malvern Zetasizer ZS instrument. Samples consisted of α-crystallin dissolved at a final concentration of 0.5 mg/mL in 10 mM phosphate-buffered saline (PBS), pH 7.4 and 6.5. Prior to analysis, all solutions were filtered through 0.22 μm pore-size syringe filters to remove dust that could interfere with the analyses. Measurements were conducted at 25 °C in disposable polystyrene

cuvettes with a 1 cm path length. Each sample was equilibrated for 3 min before data acquisition. The analysis was performed at a backscattering angle of 173°, using a 633 nm He–Ne laser. The refractive index and viscosity of the dispersant (PBS) were set to 1.334 and 0.9110 cP, respectively. Each measurement consisted of at least intensity consecutive runs per sample, and the results are reported as intensity-weighted size distributions. The polydispersity index (PdI) was also recorded to assess sample homogeneity, and in all cases it was less than or equal to 0.14. Data were processed using the Zetasizer software (Malvern Instruments, version 7.12), employing a regularized non-negative least squares (NNLS) fitting algorithm (protein analysis model).

CRediT authorship contribution statement

Damiano Calcagno: Writing – review & editing, Writing – original draft, Methodology, Investigation, Formal analysis, Data curation, Conceptualization. **Valentina Oliveri:** Investigation, Data curation. **Maria Cristina Parravano:** Resources, Project administration. **Nunzio Tuccitto:** Writing – original draft, Visualization, Supervision, Project administration, Methodology, Investigation, Formal analysis, Data curation, Conceptualization. **Giuseppe Grasso:** Writing – review & editing, Writing – original draft, Visualization, Validation, Supervision, Resources, Project administration, Methodology, Funding acquisition, Conceptualization.

Declaration of competing interest

The authors declare that they have no known competing financial interests or personal relationships that could have appeared to influence the work reported in this paper.

Acknowledgements

The authors acknowledge the Ministry of Health and Fondazione Roma for their support. This research was supported by MIUR, PRIN: P2022AW2H9 “Molecular details on the early phase of amyloid beta peptides aggregation: a multilevel approach based on carbon dots fluorescence and diffusion coefficients measurements to unveil the pathogenic molecular mechanisms at the base of Alzheimer’s disease”. The authors thank the ERMES project, funded under the European Union’s Horizon Europe – HORIZON-EIC-2024-PATHFINDEROPEN-01, grant agreement No. 101185661. Piano di incentivi per la ricerca di Ateneo 2024/2026 (Pia.ce.ri.), Università di Catania is also acknowledged.

Appendix A. Supplementary data

Supplementary data to this article can be found online at https://doi.org/10.1016/j.bios.2025.118080.

Data availability

Data will be made available on request.

References

Andley, U.P., 2007. Crystallins in the eye: function and pathology. Prog. Retin. Eye Res. 26, 78–98. https://doi.org/10.1016/j.preteyeres.2006.10.003.

Aranaz, M., Costas-Rodríguez, M., Lobo, L., García, M., González-Iglesias, H., Pereiro, R., Vanhaecke, F., 2022. Homeostatic alterations related to total antioxidant capacity, elemental concentrations and isotopic compositions in aqueous humor of glaucoma patients. Anal. Bioanal. Chem. 414, 515–524. https://doi.org/10.1007/s00216-021-03467-5.

Bajaj, A., Abutoama, M., Isaacs, S., Abuleil, M.J., Yaniv, K., Kushmaro, A., Modic, M., Cvelbar, U., Abdulhalim, I., 2023. Biofilm growth monitoring using guided wave ultralong-range surface plasmon resonance: a proof of concept. Biosens. Bioelectron. 228, 115204. https://doi.org/10.1016/j.bios.2023.115204.

Baldwin, A.J., Hilton, G.R., Lioe, H., Bagnéris, C., Benesch, J.L.P., Kay, L.E., 2011. Quaternary dynamics of αB-Crystallin as a direct consequence of localised tertiary fluctuations in the C-Terminus. J. Mol. Biol. 413, 310–320. https://doi.org/10.1016/j.jmb.2011.07.017.

Basile, G.S., Calcagno, D., Pandino, I., Pietropaolo, A., Schifino, G., Tuccitto, N., Zingale, G.A., Grasso, G., 2024. Surface plasmon resonance allows to correlate molecular properties with diffusion coefficients of linear chain alcohols. Chem. Weinh. Bergstr. Ger., e202402346 https://doi.org/10.1002/chem.202402346.

Basile, G.S., Calcagno, D., Tuccitto, N., Sbardella, D., Grasso, G., 2025. Broad-spectrum diffusion coefficient measurements via surface plasmon resonance: from thermodynamics to protein conformational disorders. ChemPhysChem 26, e202500138. https://doi.org/10.1002/cphc.202500138.

Bellia, F., Lanza, V., García-Viñuales, S., Ahmed, I.M.M., Pietropaolo, A., Iacobucci, C., Malgieri, G., D’Abrosca, G., Fattorusso, R., Nicoletti, V.G., Sbardella, D., Tundo, G. R., Coletta, M., Pirone, L., Pedone, E., Calcagno, D., Grasso, G., Milardi, D., 2019. Ubiquitin binds the amyloid β peptide and interferes with its clearance pathways. Chem. Sci. 10, 2732–2742. https://doi.org/10.1039/C8SC03394C.

Björnerås, J., Botana, A., Morris, G.A., Nilsson, M., 2014. Resolving complex mixtures: trilinear diffusion data. J. Biomol. NMR 58, 251–257. https://doi.org/10.1007/s10858-013-9752-8.

Bova, M.P., Mchaourab, H.S., Han, Y., Fung, B.K.-K., 2000. Subunit exchange of small heat shock proteins: ANALYSIS OF OLIGOMER FORMATION OF αA-CRYSTALLIN AND Hsp27 BY FLUORESCENCE RESONANCE ENERGY TRANSFER AND SITE-DIRECTED TRUNCATIONS. J. Biol. Chem. 275, 1035–1042. https://doi.org/10.1074/jbc.275.2.1035.

Calcagno, D., Perina, M.L., Distefano, A., Parravano, M., Licciardello, A., Tuccitto, N., Grasso, G., 2025. Albumin folding changes affect the microfluidic interfacial broadening revealed by surface plasmon resonance. Chem. Mater. 5, e202400034. https://doi.org/10.1002/cmtd.202400034.

Calcagno, D., Perina, M.L., Zingale, G.A., Pandino, I., Tuccitto, N., Oliveri, V., Parravano, M.C., Grasso, G., 2024. Detection of insulin oligomeric forms by a novel surface plasmon resonance-diffusion coefficient based approach. Protein Sci. Publ. Protein Soc. 33, e4962. https://doi.org/10.1002/pro.4962.

Chelius, D., Bondarenko, P.V., 2002. Quantitative profiling of proteins in complex mixtures using liquid chromatography and mass spectrometry. J. Proteome Res. 1, 317–323. https://doi.org/10.1021/pr025517j.

Cholkar, K., Dasari, S.R., Pal, D., Mitra, A.K., 2013. 1 - eye: anatomy, physiology and barriers to drug delivery. In: Mitra, A.K. (Ed.), Ocular Transporters and Receptors, Woodhead Publishing Series in Biomedicine. Woodhead Publishing, pp. 1–36. https://doi.org/10.1533/9781908818317.1.

Cottet, H., Biron, J.-P., Martin, M., 2007. Taylor dispersion analysis of mixtures. Anal. Chem. 79, 9066–9073. https://doi.org/10.1021/ac071018w.

Distefano, A., Antonio Zingale, G., Grasso, G., 2022. An SPR-Based method for hill coefficient measurements: the case of insulin-degrading enzyme. Anal. Bioanal. Chem. 414, 4793–4802. https://doi.org/10.1007/s00216-022-04122-3.

Dmitriev, A.V., Linsenmeier, R.A., 2025. pH in the vertebrate retina and its naturally occurring and pathological changes. Prog. Retin. Eye Res. 104, 101321. https://doi.org/10.1016/j.preteyeres.2024.101321.

Dreffs, A., Henderson, Desmond, Dmitriev, Andrey V., Antonetti, David A., Linsenmeier, R.A., 2018. Retinal pH and acid regulation during metabolic acidosis. Curr. Eye Res. 43, 902–912. https://doi.org/10.1080/02713683.2018.1458882.

Fu, R., Klinngam, W., Heur, M., Edman, M.C., Hamm-Alvarez, S.F., 2020. Tear proteases and protease inhibitors: potential biomarkers and disease drivers in ocular surface disease. Eye Contact Lens 46, S70. https://doi.org/10.1097/ICL.0000000000000641.

Gholami, S., Kamali, Y., Rostamzad, M.R., 2019. Glycine supplementation ameliorates retinal neuronal damage in an experimental model of diabetes in rats: a light and electron microscopic study. J. Ophthalmic Vis. Res. 14, 448–456. https://doi.org/10.18502/jovr.v14i4.5449.

Grasso, G., Bush, A.I., D’Agata, R., Rizzarelli, E., Spoto, G., 2009a. Enzyme solid-state support assays: a surface plasmon resonance and mass spectrometry coupled study of immobilized insulin degrading enzyme. Eur. Biophys. J. 38, 407–414.

Grasso, G., Mineo, P., Rizzarelli, E., Spoto, G., 2009b. MALDI, AP/MALDI and ESI techniques for the MS detection of amyloid β-peptides. Int. J. Mass Spectrom. 282, 50–55.

He, M., Luo, P., Hong, J., Wang, X., Wu, H., Zhang, R., Qu, F., Xiang, Y., Xu, W., 2019. Structural analysis of biomolecules through a combination of mobility capillary electrophoresis and mass spectrometry. ACS Omega 4, 2377–2386. https://doi.org/10.1021/acsomega.8b03224.

Homola, J., 2008. Surface plasmon resonance sensors for detection of chemical and biological species. Chem. Rev. 108, 462–493. https://doi.org/10.1021/cr068107d.

Inoue, R., Sakamaki, Y., Takata, T., Wood, K., Morishima, K., Sato, N., Okuda, A., Shimizu, M., Urade, R., Fujii, N., Sugiyama, M., 2021. Elucidation of the mechanism of subunit exchange in αB crystallin oligomers. Sci. Rep. 11, 2555. https://doi.org/10.1038/s41598-021-82250-z.

Isaacs, S., Hajoj, A., Abutoama, M., Kozlovsky, A., Golan, E., Abdulhalim, I., 2019. Resonant grating without a planar waveguide layer as a refractive index sensor. Sensors 19, 3003. https://doi.org/10.3390/s19133003.

Latunde-Dada, S., Bott, R., Hampton, K., Patel, J., Leszczyszyn, O.I., 2015. Methodologies for the taylor dispersion analysis for mixtures, aggregates and the mitigation of buffer mismatch effects. Anal. Methods 7, 10312–10321. https://doi.org/10.1039/C5AY02094H.

Lebendiker, M., 2024. Purification and quality control of recombinant proteins expressed in mammalian cells: a practical review. In: Hacker, D.L. (Ed.), Recombinant Protein Expression in Mammalian Cells: Methods and Protocols. Springer US, New York, NY, pp. 329–353. https://doi.org/10.1007/978-1-0716-3878-1_21.

Lee, H.C., Chang, T., 1996. Characterization of binary polymer mixtures by simultaneous size exclusion chromatography and interaction chromatography. Macromolecules 29, 7294–7296. https://doi.org/10.1021/ma960536y.

Lim, E.W., Fallon, R.J., Bates, C., Ideguchi, Y., Nagasaki, T., Handzlik, M.K., Joulia, E., Bonelli, R., Green, C.R., Ansell, B.R.E., Kitano, M., Polis, I., Roberts, A.J., Furuya, S., Allikmets, R., Wallace, M., Friedlander, M., Metallo, C.M., Gantner, M.L., 2024. Serine and glycine physiology reversibly modulate retinal and peripheral nerve function. Cell Metab. 36, 2315–2328.e6. https://doi.org/10.1016/j.cmet.2024.07.021.

Loukovaara, S., Sandholm, J., Aalto, K., Liukkonen, J., Jalkanen, S., Yegutkin, G.G., 2017. Deregulation of ocular nucleotide homeostasis in patients with diabetic retinopathy. J. Mol. Med. 95, 193–204. https://doi.org/10.1007/s00109-016-1472-6.

Mariani, S., Minunni, M., 2014. Surface plasmon resonance applications in clinical analysis. Anal. Bioanal. Chem. 406, 2303–2323. https://doi.org/10.1007/s00216-014-7647-5.

Masson, J.-F., 2020. Portable and field-deployed surface plasmon resonance and plasmonic sensors. Analyst 145, 3776–3800. https://doi.org/10.1039/D0AN00316F.

Midena, E., Frizziero, L., Midena, G., Pilotto, E., 2021. Intraocular fluid biomarkers (liquid biopsy) in human diabetic retinopathy. Graefes Arch. Clin. Exp. Ophthalmol. 259, 3549–3560. https://doi.org/10.1007/s00417-021-05285-y.

Moreno-Montañés, J., Blesa, J.L., 1995. IgG, albumin and total IgG index in the aqueous humour of eyes with pseudoexfoliation syndrome. Acta Ophthalmol. Scand. 73, 249–251. https://doi.org/10.1111/j.1600-0420.1995.tb00278.x.

Pan, S., Yin, L., Liu, J., Tong, J., Wang, Z., Zhao, J., Liu, X., Chen, Y., Miao, J., Zhou, Y., Zeng, S., Xu, T., 2024. Metabolomics-driven approaches for identifying therapeutic targets in drug discovery. MedComm 5, e792. https://doi.org/10.1002/mco2.792.

Peschek, J., Braun, N., Franzmann, T.M., Georgalis, Y., Haslbeck, M., Weinkauf, S., Buchner, J., 2009. The eye lens chaperone α-crystallin forms defined globular assemblies. Proc. Natl. Acad. Sci. 106, 13272–13277. https://doi.org/10.1073/pnas.0902651106.

Rajagopalan, S., Chow, C., Raghunathan, V., Fry, C.G., Cavagnero, S., 2004. NMR spectroscopic filtration of polypeptides and proteins in complex mixtures. J. Biomol. NMR 29, 505–516. https://doi.org/10.1023/B:JNMR.0000034354.30702.de.

Rasmussen, T., van de Weert, M., Jiskoot, W., Kasimova, M.R., 2011. Thermal and acid denaturation of Bovine lens α-crystallin. Proteins: Struct., Funct., Bioinf. 79, 1747–1758. https://doi.org/10.1002/prot.22998.

Sanchez, J.B.-C., Duran, M.D.P., Sáez, S.M., Ruiz, D.P., Zanon-Moreno, V., Ramos-Lopez, J.F., Galarreta-Mira, D., 2025. Correlation of biomarkers of oxidative stress and inflammation in tears and aqueous humor of primary open-angle glaucoma patients. Acta Ophthalmol. 103. https://doi.org/10.1111/aos.16969.

Shalabney, A., Lakhtakia, A., Abdulhalim, I., Lahav, A., Patzig, C., Hazek, I., Karabchevsky, A., Rauschenbach, B., Zhang, F., Xu, J., 2009. Surface plasmon resonance from metallic columnar thin films. Photonics Nanostructures - Fundam. Appl., Mediteranean Nano Photonics 2008 (MediNano-1): Devices and fabrication techiques 7, 176–185. https://doi.org/10.1016/j.photonics.2009.03.003.

Shang, F., Taylor, A., 1995. Oxidative stress and recovery from oxidative stress are associated with altered ubiquitin conjugating and proteolytic activities in Bovine lens epithelial cells. Biochem. J. 307, 297–303. https://doi.org/10.1042/bj3070297.

Shrivastav, A.M., Satish, L., Kushmaro, A., Shvalya, V., Cvelbar, U., Abdulhalim, I., 2021. Engineering the penetration depth of nearly guided wave surface plasmon resonance towards application in bacterial cells monitoring. Sensor. Actuator. B Chem. 345, 130338. https://doi.org/10.1016/j.snb.2021.130338.

Somnin, C., Chamieh, J., Saetear, P., Cottet, H., 2024. Taylor dispersion analysis using capacitively coupled contactless conductivity detector. Talanta 272, 125815. https://doi.org/10.1016/j.talanta.2024.125815.

Sprague-Piercy, M.A., Rocha, M.A., Kwok, A.O., Martin, R.W., 2021. α-Crystallins in the vertebrate eye lens: complex oligomers and molecular chaperones. Annu. Rev. Phys. Chem. 72, 143–163. https://doi.org/10.1146/annurev-physchem-090419-121428.

Stamer, W.D., Baetz, N.W., Yool, A.J., 2008. Chapter 2 ocular aquaporins and aqueous humor dynamics. In: Current Topics in Membranes, the Eye's Aqueous Humor. Academic Press, pp. 47–70. https://doi.org/10.1016/S1063-5823(08)00402-X.

Svirelis, J., Andersson, J., Stradner, A., Dahlin, A., 2022. Accurate correction of the "Bulk Response" in surface plasmon resonance sensing provides new insights on interactions involving lysozyme and poly(ethylene glycol). ACS Sens. 7, 1175–1182. https://doi.org/10.1021/acssensors.2c00273.

Tang, Q., Chen, X., 2023. Nascent proteomics: Chemical tools for monitoring newly synthesized proteins. Angew. Chem. Int. Ed. 62, e202305866. https://doi.org/10.1002/anie.202305866.

Taylor, G.I., 1953. Dispersion of soluble matter in solvent flowing slowly through a tube. Proc. R. Soc. Lond. Ser. Math. Phys. Sci. 219, 186–203. https://doi.org/10.1098/rspa.1953.0139.

Tundo, G.R., Sbardella, D., Santoro, A.M., Coletta, A., Oddone, F., Grasso, G., Milardi, D., Lacal, P.M., Marini, S., Purrello, R., Graziani, G., Coletta, M., 2020. The proteasome as a druggable target with multiple therapeutic potentialities: cutting and non-cutting edges. Pharmacol. Ther. 213, 107579. https://doi.org/10.1016/j.pharmthera.2020.107579.

Valeja, S.G., Xiu, L., Gregorich, Z.R., Guner, H., Jin, S., Ge, Y., 2015. Three dimensional liquid chromatography coupling ion exchange chromatography/hydrophobic interaction chromatography/reverse phase chromatography for effective protein separation in top-down proteomics. Anal. Chem. 87, 5363–5371. https://doi.org/10.1021/acs.analchem.5b00657.

Van den Oetelaar, P.J.M., Van Someren, P.F.H.M., Thomson, J.A., Siezen, R.J., Hoenders, H.J., 1990. A dynamic Quaternary structure of bovine .alpha.-crystallin as indicated from intermolecular exchange of subunits. Biochemistry 29, 3488–3493. https://doi.org/10.1021/bi00466a010.

Winther, B., Reubsaet, J.L.E., 2005. Application of supplementary flow in comprehensive 2D liquid chromatography combining SEC and RPC. J. Separ. Sci. 28, 477–482. https://doi.org/10.1002/jssc.200400004.

Zhai, Z., Mavridou, D., Damian, M., Mutti, F.G., Schoenmakers, P.J., Gargano, A.F.G., 2024. Characterization of complex proteoform mixtures by online nanoflow ion-exchange chromatography-native mass spectrometry. Anal. Chem. 96, 8880–8885. https://doi.org/10.1021/acs.analchem.4c01760.

Zhang, Y., Fu, X., Ping, G., 2021. Selective enrichment of low-abundance compounds in a mixture by capillary electrophoresis. J. Chromatogr. A 1635, 461737. https://doi.org/10.1016/j.chroma.2020.461737.

Zingale, G.A., Pandino, I., Calcagno, D., Perina, M.L., Tuccitto, N., Grasso, G., 2024. Label-Free Determination of Diffusion Coefficients at the Nanoscale Through Modelling of the Surface Plasmo….

Zingale, G.A., Pandino, I., Distefano, A., Tuccitto, N., Grasso, G., 2023. A novel SPR based method for measuring diffusion coefficients: from small molecules to supramolecular aggregates. Biosens. Bioelectron. X 13, 100306. https://doi.org/10.1016/j.biosx.2023.100306.